

1 **A new approach to probe the degradation of fuel catalysts under realistic conditions:**
2 **combining tests in a gas diffusion electrode setup with small angle X-ray scattering**

3
4 Johanna Schröder^{a,b}, Jonathan Quinson^c, Jacob J. K. Kirkensgaard^d, Shima Alinejad^a, Vladislav
5 A. Mints^a, Kirsten M. Ø. Jensen^c, Matthias Arenz^a

6
7 ^a Department of Chemistry and Biochemistry, University of Bern, Freiestrasse 3, 3012 Bern,
8 Switzerland

9 ^b Institute of Applied and Physical Chemistry (IAPC), Center for Environmental Research and
10 Sustainable Technology, University of Bremen, Leobener Strasse 6, 28359 Bremen, Germany

11 ^c Department of Chemistry, University of Copenhagen, Universitetsparken 5, 2100 Copenhagen,
12 Denmark

13 ^d Department of Food Science, University of Copenhagen, Rolighedsvej 26, 1958 Frederiksberg,
14 Denmark

15
16 **Abstract**

17 A new approach for efficiently investigating the degradation of fuel cell catalysts under realistic
18 conditions is presented combining accelerated stress tests (ASTs) in a gas diffusion electrode
19 (GDE) setup with small angle X-ray scattering (SAXS). GDE setups were recently introduced
20 as a novel testing tool combining the advantages of classical electrochemical cells with a three-
21 electrode setup and membrane electrode assemblies (MEAs). SAXS characterization of the
22 catalyst layer enables an evaluation of the particle size distribution of the catalyst and its
23 changes upon applying an AST. The straight-forward approach not only enables stability testing
24 of fuel cell catalysts in a comparative and reproducible manner, it also allows mechanistic
25 insights into the degradation mechanism. In contrast to standard rotating disk electrode
26 measurements or identical location microscopy, typical metal loadings for proton exchange
27 membrane fuel cells (PEMFCs), i.e. $0.2 \text{ mg}_{\text{Pt}} \text{ cm}^{-2}_{\text{geo}}$, are applied in the GDE and the
28 degradation of the overall (whole) catalyst layer is probed. For the first time, realistic
29 degradation tests can be performed comparing a set of catalysts with several repeats within
30 reasonable time. It is demonstrated that independent of the initial particle size in the pristine
31 catalyst, for ASTs simulating load cycle conditions in a PEMFC, all catalysts degrade to a more
32 or less identical particle size distribution. The presented new approach will help to pave the
33 way to develop improved PEMFC catalysts.

34

35 **Keywords**

36 Gas diffusion electrode, accelerated stress tests, small angle X-ray scattering, platinum
37 nanoparticle catalysts, fuel cell catalyst testing

38

39 **1. Introduction**

40 Proton exchange membrane fuel cells (PEMFCs) are a promising alternative to replace
41 combustion engines [1–3] with the development of fuel-cells vehicles. A key component of this
42 technology are using nanoparticles (NPs), nowadays typically Pt-alloys (e.g. PtCo in the Mirai
43 automobile from Toyota) [4–6], supported on high surface carbon as catalysts [3]. For a long
44 time, the main research focus was to improve the catalyst activity leading to the development
45 of several different types of highly active catalysts [7]. More recently, the performance at high
46 current densities and the effect of high oxygen mass transfer resistances has gained increasing
47 attention [8]. It was established that the oxygen mass transfer resistance decreases by increasing
48 the metal dispersion on the support material, i.e. the decrease in particle size of the catalyst [8].
49 However, besides a high activity, a sufficient stability of the catalysts is required for
50 applications [1,9]. Today, most degradation studies are either performed under idealized
51 conditions, or they lack statistics and comparative character. Hence an efficient, i.e. fast and
52 realistic, testing of fuel cell catalysts is needed to bridge catalyst development to their
53 application in fuel cells. Ideally the testing is not of pure descriptive behavior, but also
54 mechanistic insights are provided.

55 To simulate the use of catalysts under realistic conditions and at the same time accelerate their
56 degradation, stability investigations are performed using accelerated stress tests (AST), e.g.
57 following protocols recommended by the Fuel Cell Commercialization Conference of Japan
58 (FCCJ) [10,11]. Usually such measurements are either performed in classical electrochemical
59 cells with a three-electrode setup [12] or in membrane electrode assemblies (MEAs) [13]. Both
60 approaches have advantages and disadvantages. Classic electrochemical cells enable relatively
61 fast screening at the expense of a somewhat unrealistic “environment” (e.g. liquid electrolyte).
62 MEAs offer a more realistic “environment” but require significantly more advanced facilities
63 such as a complete hydrogen infrastructure in the laboratory. In addition, MEA testing is very
64 time consuming and therefore usually not combined with spectroscopic tools in a comparative
65 manner, i.e. comparing different catalysts and showing several repeats for each sample. A
66 powerful methodology to combine the advantages of both approaches for an efficient testing
67 fuel cell catalysts under realistic conditions is the gas diffusion electrode (GDE) setup [14,15].
68 Alinejad *et al.* [15] recently presented the benefits to perform AST protocols in gas diffusion

69 setups by following the loss in catalyst active surface area as function of the electrochemical
70 treatment.

71 In the here presented work, a significant advancement of this approach is achieved by using
72 realistic catalyst layers applied in MEA testing and by combining such tests with the analysis
73 of the catalyst layer via small angle X-ray scattering (SAXS). The known electrochemical
74 degradation mechanisms of (1) migration of particles followed by coalescence and potentially
75 sintering, (2) metal dissolution, (3) electrochemical Ostwald ripening, where large particles
76 grow at the expense of small ones, and (4) particle detachment from the support [16] have a
77 direct effect on the particle size distribution of the catalysts. The understanding of the
78 degradation mechanism is key to propose and develop mitigation strategies. Commonly, the
79 determination of the particle size is done by (scanning) transmission electron microscopy
80 ((S)TEM) and to observe the change of selected particles before and after the treatment identical
81 location (IL) (S)TEM is performed using rotating disk electrode (RDE) [16–18] or GDE setups
82 [15]. However, while (S)TEM is a local method, SAXS offers the benefits to analyze the
83 particle size distribution after performing the AST in the whole catalyst layer [19,20] and even
84 without further dismantling of the GDE as we demonstrate in the present study. In the present
85 work, load-cycle conditions were simulated in an AST protocol by applying potential steps
86 between 0.6 and 1.0 V_{RHE} in oxygen saturated atmosphere at 25 and 50 °C in a GDE setup. The
87 combination of electrochemical measurements and SAXS analysis allows to determine the loss
88 in active surface area and to relate it to a change in particle size as function of operation
89 temperature and initial NP size distribution. We demonstrate with this study that the
90 combination of GDE and SAXS is an efficient way to test fuel cell catalysts in a comparative
91 manner under realistic conditions and enable mechanistic insights into the catalyst degradation.

92

93 **2. Experimental**

94 **2.1. Chemicals, materials, and gases**

95 Ultrapure Milli-Q water (resistivity > 18.2 $M\Omega \cdot cm$, total organic carbon (TOC) < 5 ppb) from
96 a Millipore system was used for catalyst ink formation, diluting the acid, and the cleaning of
97 the GDE cell. For preparing the catalysts ink isopropanol (IPA, 99.7+ %, Alfa Aesar),
98 commercial Pt/C catalysts (TEC10E20A (1-2 nm Pt/C, 19.4 wt% Pt), TEC10E50E (2-3 nm
99 Pt/C, 46.0 wt% Pt), TEC10E50E-HT (4-5 nm Pt/C, 50.6 wt% Pt), Tanaka kikinzoku kogyo),
100 and Nafion dispersion (D1021, 10 wt. %, EW 1100, Fuel Cell Store) was used.

101 The GDE was prepared using a Nafion membrane (Nafion 117, 183 μm thick, Fuel Cell Store),
102 two gas diffusion layers (GDL) (Sigracet 39AA, 280 μm thick, Fuel Cell Store; with a

103 microporous layer (MPL): Sigracet 39BC, 325 μm thick, Fuel Cell Store). In this study the
104 Nafion membrane was always pretreated. Circles with a diameter of 2 cm were cut from a sheet
105 of Nafion membrane. Those cutoff membranes were treated in 5 wt.% H_2O_2 (Hänseler, 30 min,
106 80 $^\circ\text{C}$), rinsed with Milli-Q water, treated in Milli-Q water (30 min, 80 $^\circ\text{C}$), rinsed again with
107 Milli-Q water, and treated in 8 wt.% H_2SO_4 (30 min, 80 $^\circ\text{C}$). After final rinsing of the cutoff
108 membranes with Milli-Q water, they were kept in a glass vial filled with Milli-Q water.
109 Diluted 70 % perchloric acid (HClO_4 , 99.999 % trace metals basis, Sigma Aldrich) as
110 electrolyte and the gases Ar (99.999 %), O_2 (99.999 %), and CO (99.97 %) from Air Liquide
111 were used in the electrochemical measurements.

112

113 **2.2. Gas diffusion electrode setup**

114 An in-house gas diffusion electrode setup as described before[14,15] was used in the
115 electrochemical measurements. The GDE was placed on top of the flow field in the iron cell
116 body with the Nafion membrane upwards. The upper cell part above the Nafion membrane is
117 made of polytetrafluoroethylene (PTFE). A platinum wire was used as a counter electrode (CE)
118 and a reversible hydrogen electrode (RHE) as a reference electrode (RE). The CE was placed
119 inside a glass capillary with a glass frit on the bottom to avoid the trapping of gas bubbles in
120 the hole of the Teflon cell and hence helping to improve the reproducibility of the measurement.
121 All potentials in this study are referred to the RHE potential.

122 In an initial cleaning the Teflon upperpart was soaked in acid ($\text{H}_2\text{SO}_4:\text{HNO}_3 = 1:1$, v:v)
123 overnight. After rinsing it with ultrapure water, it was boiled twice in ultrapure water. Between
124 the measurements the Teflon upper part, the RE, and the glass capillary were boiled once in
125 ultrapure water.

126

127 **2.3. Catalyst synthesis and ink formation**

128 Three commercial Tanaka catalysts with different particle sizes and metal loadings were used.
129 The ink was formed by dispersing the catalysts in a mixture of Milli-Q water and IPA
130 (water/IPA ratio of 3:1) to obtain about 5 mL of ink with a Pt concentration of 0.5 mg mL^{-1} .
131 The mixture was sonicated for 5 min in a sonication bath to get a suitable dispersion. 23-98 μL
132 of Nafion was added (Nafion/carbon mass ratio of 1). The dispersion was again sonicated for 5
133 min in a sonication bath.

134

135

136

137 **2.4. Vacuum filtration and pressing of GDE**

138 The Sigracet 39BC gas diffusion layer (GDL) was placed in a vacuum filtration setup between
139 a glass funnel and a sand core filter. All this was placed on a collecting bottle as described by
140 Yarlagadda *et al.* [21]. 4 mL of the inks were diluted with 7 mL of Milli-Q water and 29 mL of
141 IPA (water-IPA ratio of 1:3, Pt concentration of 0.05 mg L⁻¹). The mixture was sonicated for 1
142 min. The 40 mL diluted ink were filled in a funnel. A jet water pump was used to deposit the
143 catalyst on top of the GDL. When the collected solvent was not colorless it was refilled into the
144 funnel and the vacuum filtration was started again. Afterwards, the GDE was dried at least
145 overnight on air. By this procedure a theoretical Pt loading of 0.208 mg_{Pt} cm⁻²_{geo} was generated.
146 The Nafion membrane was pressed on top of the GDE. Therefore, a Teflon sheet was placed
147 on top of a Teflon block and afterwards the GDL without MPL (Ø 2 cm), GDL with MPL (Ø 2
148 cm with hole of Ø 3 mm) and the catalyst on the GDL from the vacuum filtration (Ø 3 mm) in
149 the hole. A Nafion membrane (to avoid later the leaking of the electrolyte into the GDE) was
150 rinsed with Milli-Q water, dried and followed by a second Teflon sheet and a second Teflon
151 block placed on top. Everything was placed between two metal blocks and the pressing was
152 performed at 2 tons for 10 min.

153

154 **2.5. Electrochemical measurement**

155 The electrochemical measurements were performed with a computer controlled parallel
156 potentiostat (ECi-242, NordicElectrochemistry). Two measurements could be performed in
157 parallel by splitting the gas inlet after humidification of the gas. Hence the gas inlet of two GDE
158 setups was connected to the same bubbler. 4 M HClO₄ aqueous solution in the upper Teflon
159 compartment of the GDE setup was used as electrolyte and different temperatures (25 or 50 °C)
160 were applied using a fan in an isolated Faraday cage. Before performing the AST protocols first
161 20 cyclic voltammograms (CVs) in Argon (Ar, with a scan rate of 500 mV s⁻¹, 0.06-1.1 V_{RHE})
162 were performed to assess if the assembling of the cell was successful. For cleaning the surface,
163 afterwards CVs in oxygen (O₂) were performed: 20 CVs with 500 mV s⁻¹, then ca. 50 CVs with
164 50 mV s⁻¹ until a stable CV was obtained. The resistance between the working electrode (WE)
165 and RE (ca. 10 Ω) was compensated to around 2 Ω by using the analog positive feedback
166 scheme of the potentiostat. The resistance was determined online using an AC signal (5 kHz, 5
167 mV) [22]. Before starting the measurement, to make sure that the O₂ was completely replaced,
168 CVs in Ar (50 CVs, 500 mV s⁻¹) were done. The wished temperature for the following AST
169 was adjusted.

170 To investigate the degradation mechanism(s) of the Pt/C electrocatalysts, ASTs as reported by
 171 Alinejad *et al.* [15] were used. The applied electrode potential was stepped between 0.6 and 1.0
 172 V_{RHE} and hold for three seconds, respectively to simulate the load-cycle conditions. The surface
 173 loss of the catalysts during the AST was determined by comparing the ECSA obtained from the
 174 CO stripping voltammetry before and after the AST of at least three reproducible measurements.
 175 The ECSA values in $\text{m}^2 \text{g}_{\text{Pt}}^{-1}$ were determined using the theoretical Pt loading of $0.208 \text{ mg}_{\text{Pt}}$
 176 $\text{cm}^{-2}_{\text{geo}}$ and the surface area (in cm^2) determined by CO stripping. ASTs were performed in O_2
 177 with 9000 steps at 25°C or 5000 steps at 50°C .

178

179 **2.6. SAXS analysis**

180 A SAXSLab instrument (Niels Bohr Institute, University of Copenhagen, Denmark) equipped
 181 with a 100XL+ micro-focus sealed X-ray tube (Rigaku) producing a photon beam with a
 182 wavelength of 1.54 \AA was used for SAXS data acquisition [20,23]. A 2D 300 K Pilatus detector
 183 from Dectris was used to record the scattering patterns and the samples did not show anisotropy.
 184 The two-dimensional scattering data were azimuthally averaged, normalized by the incident
 185 radiation intensity, the sample exposure time and the transmission using the Saxsgui software.
 186 Data were then corrected for background and detector inhomogeneities using standard
 187 reduction software. Samples were sealed between two $5\text{--}7 \mu\text{m}$ thick mica windows in dedicated
 188 sample cells and measurements performed in vacuum. The background measurement was made
 189 with a GDL Sigracet 39BC without NPs.

190 The radially averaged intensity $I(q)$ is given as a function of the scattering vector $q = 4\pi \cdot \sin(\theta)/\lambda$,
 191 where λ is the wavelength and 2θ is the scattering angle. The background corrected scattering
 192 data were fitted using a power law to take into account the behavior at low q value and a model
 193 of polydisperse spheres described by a volume-weighted log-normal distribution. This model
 194 leads to satisfying results for 13 samples out of 36 samples. The remaining data were then best
 195 fitted by adding a second model of polydisperse spheres also described by a volume-weighted
 196 log-normal distribution (for 11 samples out of 36). A structure factor contribution was
 197 sometimes needed to properly model the data for the 2 polydisperse sphere models (6 samples
 198 out of 36). We employed a hard-sphere structure factor $F(R,\eta)$ as described in Reference [24].
 199 The scattering data are fitted to the following general expression:

$$200 \quad I(q) = A \cdot q^{-n} + C_1 \cdot F(R_1, \eta_1) \cdot \int P_{s1}(q, R) V_1(R) D_1(R) dR$$

$$201 \quad + C_2 \cdot \int P_{s2}(q, R) V_2(R) D_2(R) dR$$

202 where $A \cdot q^{-n}$ corresponds to the power law where A and n are free parameters; C_1 and C_2 are
203 scaling constants, Ps_1 and Ps_2 the sphere form factors, V_1 and V_2 the particle volumes and D_1
204 and D_2 the log-normal size distribution. The sphere form factor is given by:

$$205 \quad P_s(q,R) = (4\pi R^3 \frac{\sin(qR) - qR \cos(qR)}{(qR)^3})^2$$

206 and the log-normal distribution by:

$$207 \quad D(R) = \frac{1}{R\sigma\sqrt{2\pi}} \exp\left(-\frac{\left[\ln\left(\frac{R}{R_0}\right)\right]^2}{2\sigma^2}\right)$$

208 where σ is the variance and R_0 the geometric mean of the log-normal distribution. The fitting
209 was done using home written MATLAB code. The free parameters in the model are: A , n , R_1 ,
210 R_2 , σ_1 , σ_2 , C_1 , C_2 , η_1 . The values obtained for these parameters are reported in **Table S1**. In
211 most cases, i.e. 13 out of 36 samples, only 5 free parameters were needed, and a one population
212 model was enough to describe the sample. For 3 samples a model adding a structure factor with
213 6 free parameters gave a better fit. After ASTs however and in particular for the initially 1-2
214 nm Pt/C catalysts, better fits were obtained with 8 free parameters considering 2 spheres
215 populations. In 3 cases a better fit was obtained with 9 free parameters. In order to account for
216 the two populations, the reported probability density functions were weighted by the relative
217 surface contribution of the spheres as detailed in SI. The scattering data and corresponding fits
218 are reported in **Figures S1-S4 and Table S1**.

219 The “starting size” was analyzed from three samples of 3 mm diameter punched from catalyst
220 film on the GDL after vacuum filtration. Three samples with reproducible ECSAs after the AST
221 were analyzed by punching a circle with a diameter of 5 mm around the GDE (of 3 mm) with
222 the Nafion membrane on top. The background sample was obtained by performing the AST
223 protocol on a catalyst free “GDE” by using a circle with a diameter of 3 mm Sigracet 39BC as
224 “GDE” (pressing was performed the same way as before).

225

226 **2.7. TEM analysis**

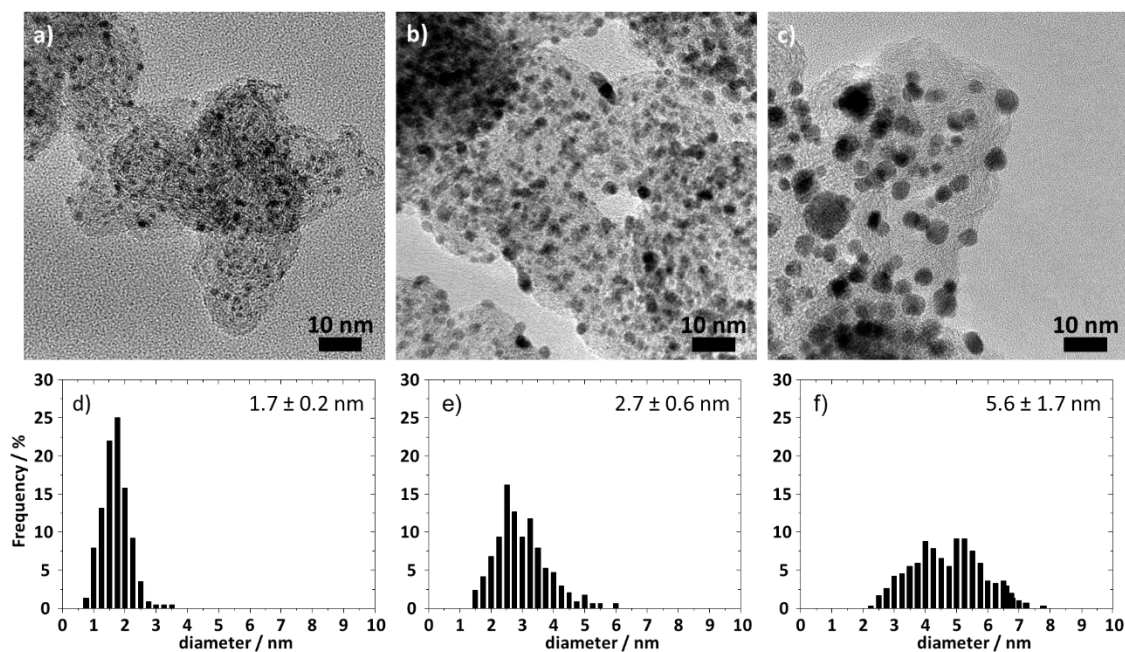
227 TEM micrographs were obtained using a Jeol 2100 operated at 200 kV. Samples were
228 characterized by imaging at least 5 different areas of the TEM grid at minimum 3 different
229 magnifications. The size (diameter) of the NPs was estimated using the imageJ software and
230 considering at least 200 NPs. The samples Pt/C were diluted in ethanol before being dropped
231 on drop casted onto a holey carbon support film of Cu 300 mesh grids (Quantifoil).

232

233 3. Results and Discussion

234 An efficient catalyst testing must be fast, performed under realistic conditions, and conducted
235 to allow several repeats for each catalyst sample. To assess the Pt NP size evolution in Pt/C
236 catalysts, SAXS is so far mainly used in combination with RDE testing in addition to the local
237 technique (S)TEM [19,20]. Although single RDE measurements are fast, the testing conditions
238 are far from the ones in fuel cell devices [14,15]; a liquid electrolyte is employed, which
239 respective type of anions [25–27] and pH values [28,29] influence Pt dissolution while the
240 catalyst film thickness (loading on the glassy carbon tip) is significantly lower than in a fuel
241 cell. Furthermore, to reach sufficient signal to noise ratios for the SAXS analysis, the catalyst
242 layer must be collected from several RDE measurements. This renders the study of the effect
243 of stability tests on the NP size impractical and time consuming. The conditions in MEA testing
244 are realistic but time consuming and rarely performed with several repeats of different catalysts.
245 Among the very few *in situ* SAXS studies reported, most require exposure of the electrocatalyst
246 to liquid electrolyte flow or are performed in a MEA [30–33]. In setups exposing the catalyst
247 to liquid electrolyte flow the risk of a mechanical delamination and incomplete catalyst
248 utilization is given. For an analysis of the catalyst layers in MEA, a dismantling is necessary to
249 avoid probing anode and cathode catalyst at the same time. These severe limitations call for
250 further improvement.

251



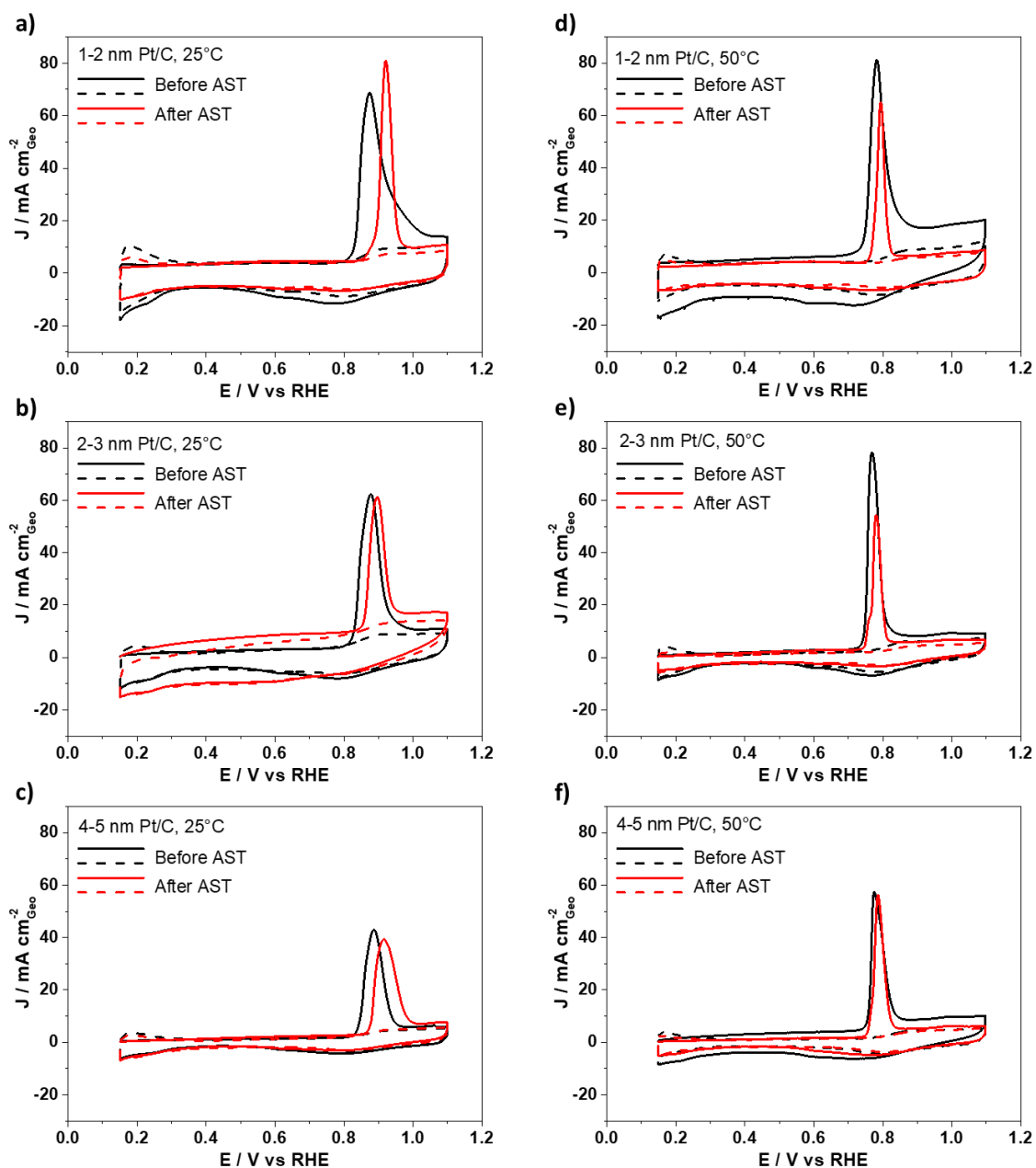
253

254 **Figure 1:** TEM micrographs and size distributions of the commercial 1-2 nm (a, d), 2-3 nm (b, e), and 4-5 nm (c, f) Pt/C catalyst powders.

255 In contrast, the GDE setup provides more realistic conditions than the RDE method but is at the
256 same time a more simple and faster methodology than flow cell or MEA measurements [14,15].
257 Therefore, in this work, a GDE setup is used to investigate the degradation of three commercial
258 Tanaka Pt/C catalysts with different NP size distributions ranging from 1-2 to 4-5 nm (hereafter
259 denoted as 1-2 nm Pt/C, 2-3 nm Pt/C, and 4-5 nm Pt/C) that are often used as benchmark
260 catalysts in RDE testing [34]. TEM micrographs of the three catalyst powders are displayed in
261 **Figure 1**. In a recent work we showed that ASTs can be performed in our GDE setup but the
262 used catalyst loading was comparable to loadings for RDE measurements and hence far from
263 realistic fuel cell loadings [15]. In the present work, the catalyst film on the GDL (i.e. the GDE)
264 is prepared by vacuum filtration as described by Yarlagadda *et al.* [21] to reach typical catalyst
265 loadings for fuel cells in cars of $0.2 \text{ mg}_{\text{Pt}} \text{ cm}^{-2}_{\text{geo}}$ [8]. ASTs are performed at 25 °C (9000 steps
266 in O₂ between 0.6 and 1.0 V_{RHE}, 3 s holding) and additionally at 50 °C (with a reduced number
267 of degradation steps to 5000 to reach a comparable loss in surface area) to generate more
268 realistic fuel cell conditions [4]. In the SI it is demonstrated that with the established procedure,
269 reproducible particle size distributions of the different Pt/C catalysts could be determined
270 before as well as after the ASTs. The same reproducibility is observed for the determined values
271 of the electrochemically active surface area (ECSA), see relatively low standard deviations in
272 **Table 1**. By analyzing the electrochemical measurements recorded in the GDE setup, (**Figure**
273 **2** and **Table 1**) and comparing the ECSA values of the catalysts with the ones reported from
274 RDE measurements in literature it is further confirmed that the catalyst layer is fully utilized
275 [34]. This is of utmost importance for the SAXS analysis, which otherwise would be misleading
276 as parts of the catalyst layer that were not be under electrochemical control would not be
277 subjected to any degradation and hence would not show any change in the particle size
278 distributions. In addition, it is observed that going from 25 °C to 50 °C, the peak potential of
279 the CO stripping is shifted to lower electrode potentials and the established initial ECSA is
280 slightly reduced (see **Figure 2** and **Table 1**). This finding is in agreement with the expected
281 effect of higher temperature reducing the equilibrium coverage of adsorbents and facilitating
282 the oxidation of CO [35]. Based on the average of the maximum particle sizes obtained from
283 SAXS data analyses “theoretical” surface areas before the AST can be calculated (see Table S3
284 in SI). Comparing the experimental ECSA established by the CO stripping and “theoretical”
285 surface areas uncovers that although large NPs have in total less surface area, a higher fraction
286 of the surface area is accessible for catalytic reactions as compared to the small NPs.
287 As prepared, the catalysts with the smaller NPs exhibit higher initial ECSA than the catalyst
288 with larger NPs (see **Table 1**). At the same time, the smaller NPs experience a larger ECSA

289 loss upon applying the AST: 43 ± 1 and 34 ± 1 % for 1-2 and 2-3 nm Pt/C, respectively as
290 compared to 4 ± 1 % for 4-5 nm Pt/C at 25°C. An increase in temperature accelerates the loss
291 in ECSA considerably (AST duration of 10 h at 50 °C as compared to 16 h 40 at 25 °C).
292 Interestingly, the 4-5 nm Pt/C catalyst is very stable. Its ECSA loss upon applying the AST is
293 very small, i.e. after more than 16 h of AST at 25 °C it is less than 5% and thus almost negligible.
294 Increasing the temperature to 50 °C, the ECSA loss increases to 16% (note that the testing time
295 was shorter, i.e. 10 h), but is still minor as compared to the ECSA loss of the 1-2 and 2-3 Pt/C
296 catalysts of 53 ± 1 and 48 ± 2 %, respectively. Another highly important observation results
297 from a comparison of the ECSA loss at 25 °C (see **Figure 2**). In our previous study by Alinejad
298 *et al.* [15], we used the same AST protocol but significantly lower catalyst loadings on the GDL.
299 With catalyst loadings typical for RDE testing [36] (i.e. ca. $8 \mu\text{g cm}^{-2}_{\text{geo}}$ vs. $0.2 \text{ mg cm}^{-2}_{\text{geo}}$ here),
300 significantly higher ECSA losses are observed, i.e. 48 ± 2 % with lower loading as compared
301 to 34 ± 1 % in this study for the 2-3 nm Pt/C catalyst and 18 ± 1 % with lower loading as
302 compared to 4 ± 1 % here for the 4-5 nm Pt/C catalyst (see **Table 1** and SI). Such dependence
303 of the degradation on the film thickness was observed previously in our laboratory in RDE
304 measurements (not published) as well as in Pt dissolution measurements determined via
305 scanning flow cell (SFC) measurements coupled to inductively coupled plasma mass
306 spectrometry (ICP-MS) [37,38]. The influence of the catalyst film thickness on the observed Pt
307 dissolutions rates was assigned to differences in the probability of re-deposition of the Pt ions
308 [37]. Comparing the GDE studies with different catalyst loading, typically resulting in different
309 film thickness, it can be concluded that although identical trends in stability of the two different
310 catalysts are observed, an extrapolation of the results to fuel cell conditions is more difficult if
311 very thin catalyst films are used since phenomena such as re-deposition of Pt ions do not occur.
312 Therefore, the here presented results highlight the importance of realistic conditions for
313 degradation studies.

314



315
 316 **Figure 2:** Representative CO stripping curves (solid lines) and subsequent cyclic
 317 voltammograms in Ar (dash lines) of commercial 1-2 nm (a,d), 2-3 nm (b, e), and 4-5 nm (c, f)
 318 Pt/C catalysts before (black lines) and after (red lines) ASTs in O₂ at 25 °C (a, b, c, 9000 steps
 319 between 0.6 and 1.0 V_{RHE}, 3 s holding) or 50 °C (d, e, f, 5000 steps between 0.6 and 1.0 V_{RHE},
 320 3 s holding).

321
 322
 323
 324

325 **Table 1:** Experimental ECSA before and after AST of commercial Pt/C catalysts at T = 25 °C
 326 (9000 steps between 0.6 and 1.0 V_{RHE}) and 50 °C (5000 steps between 0.6 and 1.0 V_{RHE}) in
 327 oxygen and determined ECSA loss after the AST of three reproducible repeats. The error
 328 indicates the standard deviation of the three measurements.

| T / °C | Pt/C catalysts | ECSA/ m ² g ⁻¹ Pt | | surface loss |
|--------|----------------|---|-----------|--------------|
| | | before AST | after AST | / % |
| 25 | 1-2 nm | 109 ± 4 | 62 ± 3 | 43 ± 1 |
| | 2-3 nm | 81 ± 1 | 54 ± 1 | 34 ± 1 |
| | 4-5 nm | 57 ± 1 | 55 ± 1 | 4 ± 1 |
| 50 | 1-2 nm | 90 ± 2 | 43 ± 2 | 53 ± 1 |
| | 2-3 nm | 67 ± 4 | 35 ± 3 | 48 ± 2 |
| | 4-5 nm | 50 ± 2 | 42 ± 1 | 16 ± 2 |

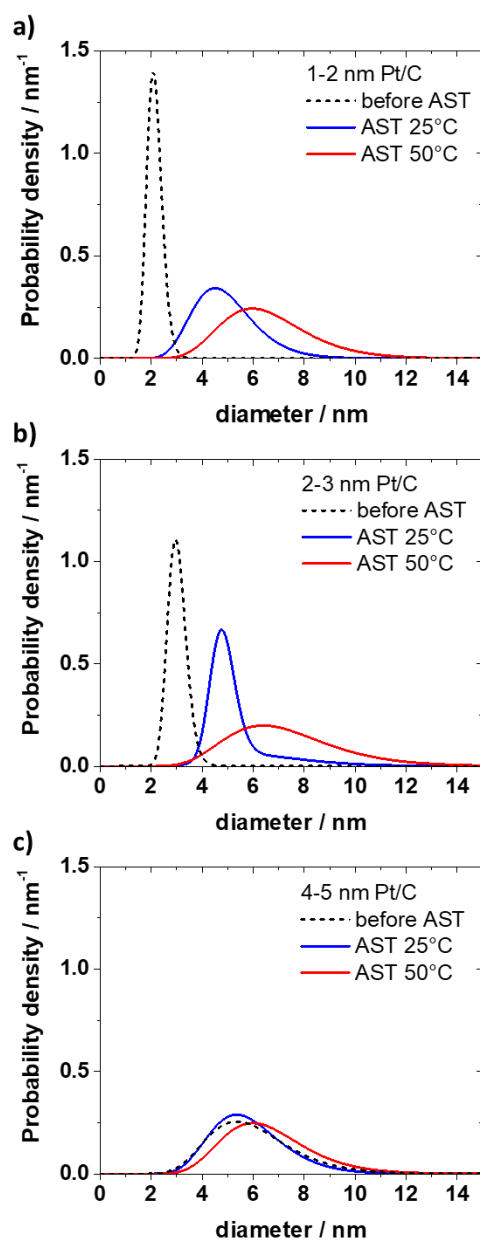
329
 330 Further, crucial mechanistic information concerning the change in the NP size distribution after
 331 applying the AST can be extracted from the SAXS data. Representative size distributions are
 332 shown in **Figure 3** and repeats in the SI. In the following we refer to the average of the mean
 333 size of the particle size distribution and the average of the deviation to compare the catalyst
 334 sizes. As a result of the AST treatments (at 25 °C or 50 °C) the size distribution (established by
 335 SAXS) of all catalysts increases as it is expected from the ECSA loss determined in the CO
 336 stripping measurements. For the 1-2 nm Pt/C catalyst the increase in size is most dramatic, an
 337 increase from 2.1 ± 0.1 to 4.6 ± 0.4 (AST in O₂ at 25 °C) and 6.0 ± 0.4 nm (AST in O₂ at 50°C)
 338 is determined, while for the 2-3 nm Pt/C catalyst an increase from 2.8 ± 0.1 to 4.9 ± 0.1 (25 °C)
 339 and 4.9 ± 1.7 nm (50 °C) is observed. Only the 4-5 nm Pt/C catalyst shows a relative moderate
 340 increase in particle size, i.e. from 5.7 ± 0.1 to 6.1 ± 0.5 (25 °C) and 6.4 ± 0.0 nm (50 °C) in line
 341 with the very moderate ECSA loss. Interestingly, after applying the AST at 50 °C the “end of
 342 treatment” particle sizes of all three Pt/C catalysts are very similar, i.e. they are all in the range
 343 of 4.9-6.4 nm. The results demonstrate that, as expected, the degradation and the particle growth
 344 are more significant for catalysts with small NPs [39].

345 More importantly, we document for the first time to the best of our knowledge that the “end of
 346 treatment” particle size of around 6 nm is rather independent from the “starting size” and the
 347 temperature, i.e. after the two AST protocols all three catalysts exhibit more or less the same
 348 size distribution. This is an important finding considering that increasing the power density in
 349 PEMFCs for mobile applications is of high priority [8]. Currently a large performance loss is

350 observed at high-current density ($> 1 \text{ A cm}^{-2}$) and it is proposed that a resistive oxygen mass
351 transfer term can be addressed among others through high and stable Pt dispersion (i.e. small
352 NPs) [8]. Our results indicate a serious limitation for such efforts to decrease oxygen mass
353 transfer resistances by increasing the catalyst dispersion (i.e. NP size) unless strategies are
354 found and successfully implemented to inhibit the growth in particle size under operation. At
355 the same time the presented GDE methodology provides an easy means to screen test the
356 behavior of different catalysts under realistic conditions.

357 Focusing on the degradation mechanism, the observed particle size distribution after
358 degradation reported in **Figure 3** is consistent with the established loss in surface area (see
359 **Table 1**). While the surface loss could be in general a consequence of all degradation
360 mechanisms (migration/coalescence, metal dissolution, Ostwald ripening, particle detachment),
361 the observed increase in particle size can occur due to electrochemical Ostwald ripening and
362 particle coalescence. The dependence of the degradation (ECSA loss) on the catalyst layer
363 thickness (catalyst loading on GDL) indicates a significant contribution of electrochemical
364 Ostwald ripening. However, the tail of the size distributions to large sizes (maximum at small
365 size) after the AST at $25 \text{ }^\circ\text{C}$ could be an indication for coalescence [40], while tailing to small
366 NP sizes (maximum at large size) after the AST at $50 \text{ }^\circ\text{C}$ could signify Ostwald ripening [41,42].
367 The shoulder in the particle size distribution after the AST at $25 \text{ }^\circ\text{C}$ for 2-3 nm Pt/C, consistent
368 with the “end of treatment size” after the AST at $50 \text{ }^\circ\text{C}$, on the other hand might be an indication
369 for coalescence followed by Ostwald ripening into spherical particles under the AST treatment
370 and therefore coalescence might be difficult to detect in the “end of treatment” catalyst. Such a
371 simultaneous occurrence of both growth mechanisms complicates the interpretation of the tailed
372 size distributions [13] and the results do not allow an unambiguous separation of Ostwald
373 ripening and coalescence. Particle detachment, by comparison, leads to a loss in surface area
374 while maintaining the size distribution [43]; a scenario that would best fit to the behavior of the
375 4-5 nm Pt/C catalyst, but certainly not for the other two catalysts. Mayrhofer *et al.* [43] showed
376 in IL-TEM that the main degradation mechanism of the 4-5 nm Pt/C catalyst at room
377 temperature and exposure to liquid electrolyte is particle detachment. However, at this point the
378 occurrence of particle detachment in the GDE setup cannot be proven. Metal dissolution
379 (without re-deposition) would lead to a decrease in particle size and is not observed in any of
380 the Pt/C catalysts, i.e. the determined size distributions exhibit very low probability towards
381 small particle sizes. A deposition of the dissolved Pt-ions in the Nafion membrane as observed
382 in MEA measurements seems unlikely, as in the MEA the process is caused by the hydrogen
383 gas crossover [13]. In the GDE measurements, a hydrogen gas crossover through the Nafion

384 membrane is not expected as the measured gas flow at the gas inlet and outlet are constant and
385 the electrolyte above the membrane is not purged with hydrogen. Therefore, more likely this
386 observation might be related to a (small) component of loss in surface area due to particle
387 detachment.
388



389
390 **Figure 3:** Representative SAXS particle size distributions of commercial 1-2 nm (a), 2-3 nm
391 (b), and 4-5 nm (c) Pt/C catalyst before (dash black lines) and after ASTs in O_2 at 25 °C (blue
392 lines, 9000 steps between 0.6 and 1.0 V_{RHE} , 3 s holding) or 50 °C (red lines, 5000 steps
393 between 0.6 and 1.0 V_{RHE} , 3 s holding).
394

395 **4. Conclusion**

396 In summary, in the present work we demonstrate the strength of the application of GDE setups
397 - as compared to classical electrochemical cells or MEAs - for the investigation of catalyst
398 degradation under realistic conditions. In the GDE setup, only one half-cell reaction of a fuel
399 cell, e.g. the oxygen reduction reaction (ORR), is investigated, thus separating anode and
400 cathode degradation. Without further disassembling (as opposed to MEA measurements) or
401 sample collection (in contrast to RDE measurements), the catalyst layer can be investigated by
402 SAXS measurements even without removing the Nafion membrane.

403 Applying conditions close to MEA testing (regarding the setup [15], loading [8], and
404 temperature [4]) the degradation mechanism can be analyzed based on the change in the size
405 distribution and the ECSA obtained by CO stripping. It is found that after applying the ASTs,
406 catalysts with small NPs exhibit significant degradation and particle growth. While this is an
407 expected result, comparing the investigations with previous ones, it is found that the amount of
408 degradation depends on the film thickness; thin films exhibit more degradation than thicker
409 films. The main mechanism seems particle growth based on either coalescence and/or
410 electrochemical Ostwald ripening whereas only for the 4-5 Pt/C catalyst there is a weak
411 indication of particle loss at the applied conditions. The here introduced combination of GDE
412 and SAXS offers a straight-forward way for comparative studies of the degradation of several
413 different fuel cell catalysts with significant advantages over RDE and MEA measurements and
414 thus will aid the quest for developing improved PEMFC catalysts.

415

416 **Acknowledgments**

417 This work was supported by the Swiss National Science Foundation (SNSF) via the project
418 No. 200021_184742. J.S. acknowledges the German Research Foundation (DFG) for
419 financial support (KU 3152/6-1) and the German Academic Exchange Service (DAAD) for
420 financial support through a scholarship for an academic exchange to the University of Bern.
421 J.Q and K.M.Ø.J thank the Villum foundation for financial support through a Villum Young
422 Investigator grant. J.Q. and M.A. thank Dr Luise Theil Kuhn and Dr Søren B. Simonsen,
423 technical University of Denmark (DTU) for access to TEM facilities. J.Q., K.M.Ø.J. and
424 J.J.K.K. acknowledge local support and continued access to the University of Copenhagen
425 SAXSLab facility.

426

427

428

429 **Authors information**

430 **Contribution**

431 J.S. and M.A. designed the electrochemical experiments, which were prepared and performed
432 by J.S. J.S. prepared the samples for SAXS measurements and participated in the SAXS data
433 analysis. J.Q. performed the TEM and SAXS measurements and analysis. J.J.K.K. supervised
434 the SAXS data acquisition and analysis. S.A. gave advices for the GDE preparation, provided
435 surface area data for low loading GDE and participated in the discussion of the GDE results.
436 V.M. gave advice for the vacuum filtration and the GDE preparation. M.A. and K.M.Ø.J.
437 supervised the research. J.S. and M.A. wrote the first draft of the paper, which was read and
438 commented by all authors.

439

440 **Competing interests**

441 The authors declare no competing interests.

442

443 **References**

- 444 [1] I. Katsounaros, S. Cherevko, A.R. Zeradjanin, K.J.J.J. Mayrhofer, Oxygen
445 electrochemistry as a cornerstone for sustainable energy conversion, *Angew. Chemie -*
446 *Int. Ed.* 53 (2014) 102–121. <https://doi.org/10.1002/anie.201306588>.
- 447 [2] T. Reier, Z. Pawolek, S. Cherevko, M. Bruns, T. Jones, D. Teschner, S. Selve, A.
448 Bergmann, H.N. Nong, R. Schlögl, K.J.J. Mayrhofer, P. Strasser, Molecular insight in
449 structure and activity of highly efficient, low-Ir Ir-Ni oxide catalysts for
450 electrochemical water splitting (OER), *J. Am. Chem. Soc.* 137 (2015) 13031–13040.
451 <https://doi.org/10.1021/jacs.5b07788>.
- 452 [3] M.K. Debe, Electrocatalyst approaches and challenges for automotive fuel cells,
453 *Nature.* 486 (2012) 43–51. <https://doi.org/10.1038/nature11115>.
- 454 [4] T. Yoshida, K. Kojima, Toyota MIRAI Fuel Cell Vehicle and Progress Toward a
455 Future Hydrogen Society, *Electrochem. Soc. Interface.* 24 (2015) 45–49.
456 <https://doi.org/10.1149/2.F03152if>.
- 457 [5] V.R. Stamenkovic, B.S. Mun, M. Arenz, K.J.J. Mayrhofer, C.A. Lucas, G. Wang, P.N.
458 Ross, N.M. Markovic, Trends in electrocatalysis on extended and nanoscale Pt-
459 bimetallic alloy surfaces, *Nat. Mater.* 6 (2007) 241–247.
460 <https://doi.org/10.1038/nmat1840>.
- 461 [6] D. Wang, H.L. Xin, R. Hovden, H. Wang, Y. Yu, D.A. Muller, F.J. Disalvo, H.D.
462 Abreuña, Structurally ordered intermetallic platinum-cobalt core-shell nanoparticles

- 463 with enhanced activity and stability as oxygen reduction electrocatalysts, *Nat. Mater.*
464 12 (2013) 81–87. <https://doi.org/10.1038/nmat3458>.
- 465 [7] B. Han, C.E. Carlton, A. Kongkanand, R.S. Kukreja, B.R. Theobald, L. Gan, R.
466 O'Malley, P. Strasser, F.T. Wagner, Y. Shao-Horn, Record activity and stability of
467 dealloyed bimetallic catalysts for proton exchange membrane fuel cells, *Energy*
468 *Environ. Sci.* 8 (2015) 258–266. <https://doi.org/10.1039/c4ee02144d>.
- 469 [8] A. Kongkanand, M.F. Mathias, The Priority and Challenge of High-Power
470 Performance of Low-Platinum Proton-Exchange Membrane Fuel Cells, *J. Phys. Chem.*
471 *Lett.* 7 (2016) 1127–1137. <https://doi.org/10.1021/acs.jpcclett.6b00216>.
- 472 [9] A. Marcu, G. Toth, S. Kundu, L.C. Colmenares, R.J. Behm, Ex situ testing method to
473 characterize cathode catalysts degradation under simulated start-up/shut-down
474 conditions - A contribution to polymer electrolyte membrane fuel cell benchmarking, *J.*
475 *Power Sources.* 215 (2012) 266–273. <https://doi.org/10.1016/j.jpowsour.2012.05.010>.
- 476 [10] A. Ohma, K. Shinohara, A. Iiyama, T. Yoshida, A. Daimaru, Membrane and catalyst
477 performance targets for automotive fuel cells by FCCJ membrane, catalyst, MEA WG,
478 in: *ECS Trans.*, The Electrochemical Society, 2011: pp. 775–784.
479 <https://doi.org/10.1149/1.3635611>.
- 480 [11] Y.C. Park, K. Kakinuma, M. Uchida, D.A. Tryk, T. Kamino, H. Uchida, M. Watanabe,
481 Investigation of the corrosion of carbon supports in polymer electrolyte fuel cells using
482 simulated start-up/shutdown cycling, *Electrochim. Acta.* 91 (2013) 195–207.
483 <https://doi.org/10.1016/j.electacta.2012.12.082>.
- 484 [12] T. Nagai, H. Murata, Y. Morimoto, Influence of Experimental Conditions on the
485 Catalyst Degradation in the Durability Test, *J. Electrochem. Soc.* (2014).
486 <https://doi.org/10.1149/2.109406jes>.
- 487 [13] P.J. Ferreira, G.J. la O', Y. Shao-Horn, D. Morgan, R. Makharia, S. Kocha, H.A.
488 Gasteiger, Instability of Pt/C Electrocatalysts in Proton Exchange Membrane Fuel
489 Cells, *J. Electrochem. Soc.* 152 (2005) A2256. <https://doi.org/10.1149/1.2050347>.
- 490 [14] M. Inaba, A.W. Jensen, G.W. Sievers, M. Escudero-Escribano, A. Zana, M. Arenz,
491 Benchmarking high surface area electrocatalysts in a gas diffusion electrode:
492 measurement of oxygen reduction activities under realistic conditions, *Energy Environ.*
493 *Sci.* 11 (2018) 988–994. <https://doi.org/10.1039/C8EE00019K>.
- 494 [15] S. Alinejad, M. Inaba, J. Schröder, J. Du, J. Quinson, A. Zana, M. Arenz, Testing fuel
495 cell catalysts under more realistic reaction conditions: accelerated stress tests in a gas
496 diffusion electrode setup, *J. Phys. Energy.* 2 (2020) 024003.

- 497 <https://doi.org/10.1088/2515-7655/ab67e2>.
- 498 [16] J.C. Meier, C. Galeano, I. Katsounaros, A.A. Topalov, A. Kostka, F. Schüth, K.J.J.
499 Mayrhofer, Degradation mechanisms of Pt/C fuel cell catalysts under simulated start-
500 stop conditions, *ACS Catal.* 2 (2012) 832–843. <https://doi.org/10.1021/cs300024h>.
- 501 [17] K. Hartl, M. Hanzlik, M. Arenz, IL-TEM investigations on the degradation mechanism
502 of Pt/C electrocatalysts with different carbon supports, *Energy Environ. Sci.* 4 (2011)
503 234–238. <https://doi.org/10.1039/c0ee00248h>.
- 504 [18] A. Zana, J. Speder, M. Roefzaad, L. Altmann, M. Baumer, M. Arenz, Probing
505 Degradation by IL-TEM: The Influence of Stress Test Conditions on the Degradation
506 Mechanism, *J. Electrochem. Soc.* 160 (2013) F608–F615.
507 <https://doi.org/10.1149/2.078306jes>.
- 508 [19] J. Speder, A. Zana, I. Spanos, J.J.K. Kirkensgaard, K. Mortensen, M. Hanzlik, M.
509 Arenz, Comparative degradation study of carbon supported proton exchange membrane
510 fuel cell electrocatalysts - The influence of the platinum to carbon ratio on the
511 degradation rate, *J. Power Sources.* 261 (2014) 14–22.
512 <https://doi.org/10.1016/j.jpowsour.2014.03.039>.
- 513 [20] J. Speder, L. Altmann, M. Roefzaad, M. Bäumer, J.J.K. Kirkensgaard, K. Mortensen,
514 M. Arenz, Pt based PEMFC catalysts prepared from colloidal particle suspensions-a
515 toolbox for model studies, *Phys. Chem. Chem. Phys.* 15 (2013) 3602–3608.
516 <https://doi.org/10.1039/c3cp50195g>.
- 517 [21] V. Yarlagadda, S.E. McKinney, C.L. Keary, L. Thompson, B. Zulevi, A. Kongkanand,
518 Preparation of PEMFC Electrodes from Milligram-Amounts of Catalyst Powder, *J.*
519 *Electrochem. Soc.* 164 (2017) F845–F849. <https://doi.org/10.1149/2.1461707jes>.
- 520 [22] G.K.H. Wiberg, K.J.J. Mayrhofer, M. Arenz, Investigation of the oxygen reduction
521 activity on silver - A rotating disc electrode study, *Fuel Cells.* 10 (2010) 575–581.
522 <https://doi.org/10.1002/fuce.200900136>.
- 523 [23] J. Quinson, M. Inaba, S. Neumann, A.A. Swane, J. Bucher, S.B. Simonsen, L. Theil
524 Kuhn, J.J.K. Kirkensgaard, K.M. Jensen, M. Oezaslan, S. Kunz, M. Arenz,
525 Investigating Particle Size Effects in Catalysis by Applying a Size-Controlled and
526 Surfactant-Free Synthesis of Colloidal Nanoparticles in Alkaline Ethylene Glycol:
527 Case Study of the Oxygen Reduction Reaction on Pt, *ACS Catal.* 8 (2018) 6627–6635.
528 <https://doi.org/10.1021/acscatal.8b00694>.
- 529 [24] T. Zemb, P. Lindner, Neutron, X-rays and Light. Scattering Methods Applied to Soft
530 Condensed Matter, 1st Editio, Elsevier, Amsterdam, 2002.

- 531 [25] S. Mitsushima, Y. Koizumi, S. Uzuka, K.I. Ota, Dissolution of platinum in acidic
532 media, *Electrochim. Acta.* 54 (2008) 455–460.
533 <https://doi.org/10.1016/j.electacta.2008.07.052>.
- 534 [26] J. Omura, H. Yano, M. Watanabe, H. Uchida, Electrochemical Quartz Crystal
535 Microbalance Analysis of the Oxygen Reduction Reaction on Pt-Based Electrodes. Part
536 1: Effect of Adsorbed Anions on the Oxygen Reduction Activities of Pt in HF, HClO
537 ₄, and H₂SO₄ Solution, *Langmuir.* 27 (2011) 6464–6470.
538 <https://doi.org/10.1021/la200694a>.
- 539 [27] T.J. Schmidt, U.A. Paulus, H.A. Gasteiger, R.J. Behm, The oxygen reduction reaction
540 on a Pt/carbon fuel cell catalyst in the presence of chloride anions, *J. Electroanal.*
541 *Chem.* 508 (2001) 41–47. <https://doi.org/10.1016/j.ijhydene.2011.12.040>.
- 542 [28] Y. Furuya, T. Mashio, A. Ohma, M. Tian, F. Kaveh, D. Beauchemin, G. Jerkiewicz,
543 Influence of Electrolyte Composition and pH on Platinum Electrochemical and/or
544 Chemical Dissolution in Aqueous Acidic Media, *ACS Catal.* 5 (2015) 2605–2614.
545 <https://doi.org/10.1021/cs5016035>.
- 546 [29] A.A. Topalov, S. Cherevko, A.R. Zeradjanin, J.C. Meier, I. Katsounaros, K.J.J.
547 Mayrhofer, Towards a comprehensive understanding of platinum dissolution in acidic
548 media, *Chem. Sci.* 5 (2014) 631–638. <https://doi.org/10.1039/c3sc52411f>.
- 549 [30] K.N. Wood, S.T. Christensen, S. Pylypenko, T.S. Olson, A.A. Dameron, K.E. Hurst,
550 H.N. Dinh, T. Gennett, R. O’hayre, In situ small-angle x-ray scattering analysis of
551 improved catalyst—support interactions through nitrogen modification, *MRS*
552 *Commun.* 2 (2012) 85–89. <https://doi.org/10.1557/mrc.2012.13>.
- 553 [31] T. Binninger, E. Fabbri, A. Patru, M. Garganourakis, J. Han, D.F. Abbott, O. Sereda,
554 R. Kötz, A. Menzel, M. Nachttegaal, T.J. Schmidt, Electrochemical flow-cell setup for
555 in situ X-ray Investigations: I. Cell for SAXS and XAS at synchrotron facilities, *J.*
556 *Electrochem. Soc.* 163 (2016) H906–H912. <https://doi.org/10.1149/2.0201610jes>.
- 557 [32] M. Povia, J. Herranz, T. Binninger, M. Nachttegaal, A. Diaz, J. Kohlbrecher, D.F.
558 Abbott, B.J. Kim, T.J. Schmidt, Combining SAXS and XAS to Study the Operando
559 Degradation of Carbon-Supported Pt-Nanoparticle Fuel Cell Catalysts, *ACS Catal.* 8
560 (2018) 7000–7015. <https://doi.org/10.1021/acscatal.8b01321>.
- 561 [33] J.A. Gilbert, N.N. Kariuki, R. Subbaraman, A.J. Kropf, M.C. Smith, E.F. Holby, D.
562 Morgan, D.J. Myers, In situ anomalous small-angle x-ray scattering studies of platinum
563 nanoparticle fuel cell electrocatalyst degradation, *J. Am. Chem. Soc.* 134 (2012)
564 14823–14833. <https://doi.org/10.1021/ja3038257>.

- 565 [34] M. Nesselberger, S. Ashton, J.C. Meier, I. Katsounaros, K.J.J. Mayrhofer, M. Arenz,
566 The particle size effect on the oxygen reduction reaction activity of Pt catalysts:
567 Influence of electrolyte and relation to single crystal models, *J. Am. Chem. Soc.* 133
568 (2011) 17428–17433. <https://doi.org/10.1021/ja207016u>.
- 569 [35] E. Herrero, J.M. Feliu, S. Blais, Z. Radovic-Hrapovic, G. Jerkiewicz, Temperature
570 dependence of CO chemisorption and its oxidative desorption on the Pt(111) electrode,
571 *Langmuir*. 16 (2000) 4779–4783. <https://doi.org/10.1021/la9907432>.
- 572 [36] M. Inaba, J. Quinson, M. Arenz, pH matters: The influence of the catalyst ink on the
573 oxygen reduction activity determined in thin film rotating disk electrode
574 measurements, *J. Power Sources*. 353 (2017) 19–27.
575 <https://doi.org/10.1016/j.jpowsour.2017.03.140>.
- 576 [37] G.P. Keeley, S. Cherevko, K.J.J. Mayrhofer, The Stability Challenge on the Pathway to
577 Low and Ultra-Low Platinum Loading for Oxygen Reduction in Fuel Cells,
578 *ChemElectroChem*. 3 (2016) 51–54. <https://doi.org/10.1002/celec.201500425>.
- 579 [38] O. Kasian, S. Geiger, K.J.J. Mayrhofer, S. Cherevko, Electrochemical On-line ICP-MS
580 in Electrocatalysis Research, *Chem. Rec.* 19 (2019) 2130–2142.
581 <https://doi.org/10.1002/tcr.201800162>.
- 582 [39] E.F. Holby, W. Sheng, Y. Shao-Horn, D. Morgan, Pt nanoparticle stability in PEM fuel
583 cells: Influence of particle size distribution and crossover hydrogen, *Energy Environ.*
584 *Sci.* 2 (2009) 865–871. <https://doi.org/10.1039/b821622n>.
- 585 [40] C.G. Granqvist, R.A. Buhrman, Ultrafine metal particles, *J. Appl. Phys.* 47 (1976)
586 2200–2219. <https://doi.org/10.1063/1.322870>.
- 587 [41] A. Baldan, Progress in Ostwald ripening theories and their applications to the γ' -
588 precipitates in nickel-base superalloys Part II: Nickel-base superalloys, *J. Mater. Sci.*
589 37 (2002) 2379–2405. <https://doi.org/10.1023/A:1015408116016>.
- 590 [42] Y. Zhai, H. Zhang, D. Xing, Z.G. Shao, The stability of Pt/C catalyst in H₃PO₄/PBI
591 PEMFC during high temperature life test, *J. Power Sources*. 164 (2007) 126–133.
592 <https://doi.org/10.1016/j.jpowsour.2006.09.069>.
- 593 [43] K.J.J. Mayrhofer, J.C. Meier, S.J. Ashton, G.K.H. Wiberg, F. Kraus, M. Hanzlik, M.
594 Arenz, Fuel cell catalyst degradation on the nanoscale, *Electrochem. Commun.* 10
595 (2008) 1144–1147. <https://doi.org/10.1016/j.elecom.2008.05.032>.
- 596